

A Robustness Evaluation Method for the Robust Control of Electrical Drive Systems based on Six-sigma Methodology

Nabil Farah, Gang Lei, *Senior Member, IEEE*, Jianguo Zhu, *Senior Member, IEEE*, and Youguang Guo, *Senior Member, IEEE*

Abstract—Numerous uncertainties in practical production and operation can seriously affect the drive performance of permanent magnet synchronous machines (PMSMs). Various robust control methods have been developed to mitigate or eliminate the effects of these uncertainties. However, the robustness to uncertainties of electrical drive systems has not been clearly defined. No systemic procedures have been proposed to evaluate a control system's robustness (how robust it is). This paper proposes a systemic method for evaluating control systems' robustness to uncertainties. The concept and fundamental theory of robust control are illustrated by considering a simple uncertain feedback control system. The effects of uncertainties on the control performance and stability are analyzed and discussed. The concept of design for six-sigma (a robust design method) is employed to numerically evaluate the robustness levels of control systems. To show the effectiveness of the proposed robustness evaluation method, case studies are conducted for second-order systems, DC motor drive systems, and PMSM drive systems. Besides the conventional predictive control of PMSM drive, three different robust predictive control methods are evaluated in terms of two different parametric uncertainty ranges and three application requirements against parametric uncertainties.

Index Terms—Permanent magnet synchronous machines (PMSMs), Predictive control, Uncertainties, Robustness evaluation, Robust control, Six-sigma.

NOMENCLATURE

R_s	Stator resistance
Ψ_{pm}	Permanent magnet flux linkage
Ψ_d	Direct axis flux
Ψ_q	Quadrature axis flux
L_d, L_q	d- and q-axis inductances
v_d, v_q	d- and q-axis voltages
i_d, i_q	d- and q-axis currents
T_e	Electromagnetic torque

Manuscript received December 15, 2024; revised March 10, 2025; accepted March 27, 2025. Date of publication June 25, 2025; Date of current version April 22, 2025.

N. Farah, G. Lei, and Y. Guo are with the School of Electrical and Data Engineering, University of Technology Sydney, NSW 2007, Australia (email: nabil.farah@uts.edu.au; gang.lei@uts.edu.au; youguang.guo-1@uts.edu.au).

J. Zhu is with the School of Electrical and Information Engineering, University of Sydney, NSW 2006, Australia (e-mail: jianguo.zhu@sydney.edu.au).

(Corresponding author: N. Farah)

Digital Object Identifier 10.30941/CESTEMS.2025.00011

ω	Machine speed
B	Friction
P	Number of pole pairs
J	Motor inertia
T_{rip}	Torque ripples
i_{arip}	Stator current (i_a) ripples
X_i	Uncertain parameter
Δ_u	Unmodelled dynamics
W_u	Unmodelled dynamics weight
μ	Mean
σ	Standard deviation
USL	Upper specification limit
LSL	Lower specification limit
POF	Probability of failure
Z	Z-value
Φ	Cumulative distribution function
Φ^{-1}	Inverse transformation of a standard cumulative distribution function
n_{sys}	Sigma level of system performance
Δ_M	Manufacturing variation
Δ_O	Operational variation

I. INTRODUCTION

THE development of a control system for a specific real plant requires an approximate mathematical model of that plant to enable the design of suitable controllers based on system requirements. However, this model never accurately describes the dynamic behavior of the real plant, where some plant dynamics are not captured in the model [1]. Additionally, the system parameters are typically determined and measured under specific operating conditions and remain fixed. However, they can vary in response to variations in the system's operation, environment, or structure. These missing (unmodelled) dynamics and system parameter variations are collectively termed control system uncertainties. Such uncertainties can significantly degrade the system's performance and even lead to instability. Consequently, the concept of robust control emerged to address the design of control methods capable of handling these uncertainties effectively [2].

AC machine drives are pivotal in modern motion control systems due to their high efficiency and power capabilities. Specifically, permanent magnet synchronous machine (PMSM) drives have garnered significant attention, leading to the development of advanced control techniques such as

model predictive control (MPC) [3]-[4]. However, the performance of PMSM drives can be adversely affected by numerous uncertainties, including unmodeled dynamics and parameter variations due to material diversity, manufacturing tolerances, and changing operating conditions [5]-[6]. These uncertainties often result in unsatisfactory performance characterized by high torque and current fluctuations, as well as slow dynamic responses. A survey of PMSM drive's uncertainties and their estimations and attenuation techniques is presented in [7].

PMSM drive uncertainties are generated from diverse sources, including manufacturing and operational sources [7]. Each uncertainty can be estimated within a bounded range based on the machine structure (e.g., manufacturing tolerance) and the expected operating conditions (e.g., rated, and maximum temperature). To effectively evaluate the robustness of control methods, realistic and practical uncertainty ranges must be considered instead of random uncertainty values, such as a 200% error in specific parameters, which is unrealistic and unlikely to occur in practical situations.

Aiming to achieve the desired performance and robustness, various robust and adaptive control mechanisms are incorporated into the conventional MPC of PMSM drives to obtain robust predictive control (RPC). For example, the prediction error is included in the prediction stage to compensate for the effects of uncertainties [8]-[11]. Various observers, such as disturbance observer [12]-[13], extended state observer (ESO) [14]-[15], and sliding mode observer [16]-[17], are employed to deal with uncertainties and enhance the robustness. In addition, combining predictive control with other control techniques can form a variety of RPC methods, such as MPC with deadbeat solution [18], and repetitive control [19].

Recently, model-free predictive control (MFPC) has emerged as a promising RPC for PMSM drives. MFPC eliminates the prediction dependency on a simplified parametric machine model by developing a prediction model independent of the machine model and parameters. Using an ultra-local model [13], various MFPCs have been introduced for PMSMs with different estimation techniques of the model unknowns based on the system input and output data [20]-[21]. In addition, MFPCs can be achieved by solely using the current and previous system input and output data and their variations [22]-[23].

The robustness of most existing RPC methods is judged by evaluating performance with a few uncertain situations (e.g., parameters mismatching). For instance, the robustness of RPCs proposed in [8], [16], and [20] was assessed by applying random mismatching parameters and observing the effect on the performance. In addition, [24] and [22] evaluated the performance robustness by computing some performance measures (e.g., current ripples) with a few cases of mismatching machine resistance, inductance, or permanent magnet (PM) flux. These evaluations may have initially assessed the controller's robustness to parametric uncertainties. However, it only evaluates the controller's

performance with deterministic sets of single parametric uncertainties. It is inadequate to judge the robustness of a controller subject to stochastic multi-parametric uncertainties.

The current techniques for evaluating robustness in control systems lack a comprehensive discussion on uncertainties and their impact on robustness. Different control methods exhibit varying degrees of robustness to uncertainties, yet there is no systematic procedure for evaluating and quantifying this aspect. This becomes particularly crucial when selecting a controller for applications that require high precision (e.g., aircraft and medical equipment), as an exact robustness index is necessary. Therefore, control engineers need a quantitative robustness evaluation approach to accurately select an appropriate controller that can effectively meet the robustness level of their application.

The six-sigma methodology is a widely used quantitative quality measure that aims to improve process efficiency and effectiveness by reducing the number of defects and probability of failure (POF) [25]. In the context of PMSM drives, this methodology has been applied in [26]-[27], and [28] for design parameter optimization, primarily at the machine level, to meet the required quality standards. However, these efforts lacked an assessment of control system robustness in relation to diverse quality indicators and application requirements. Furthermore, they did not comprehensively address the scope of uncertainties or provide a clear and systematic comparison of the robustness levels among different control systems.

This research presents a clear and systematic method for evaluating the robustness of control systems. The concept of robust control and the effects of uncertainties on performance and stability are illustrated. Based on the six-sigma methodology, a robustness evaluation method is proposed to evaluate and quantify the robustness of control systems. Unlike [26]-[28], the proposed method provides a systemic and straightforward tool to obtain the robustness index of a control system to bounded uncertainty ranges. It illustrates the process of selecting various quality indicators and defining their acceptance levels (specification limits) based on different application requirements.

The proposed method serves as a valuable tool for control engineers. It empowers them to readily assess controller robustness systemically, enhancing their ability to determine and compare controller robustness and select the appropriate controller to satisfy the required quality index of their target applications.

In summary, the contributions of this paper are:

- 1) Description, modeling, and analysis of control system uncertainties and their effects on system performance are presented. The concept of robustness is clearly illustrated by considering a simple closed-loop control system.

- 2) A robustness evaluation method based on the six-sigma concept is proposed. A control system's robustness index or sigma level can be determined by defining specific indicators and evaluating the control system against them for n -samples within bounded realistic and practical parametric uncertainty ranges based on manufacturing and operational sources.

3) The proposed method is validated based on two case studies. The first case evaluates the performance and stability robustness of second-order and DC motor drive systems against parametric uncertainties. The second case evaluates the performance robustness of MPC and three existing RPC methods for PMSMs. Their robustness indexes (sigma levels) are obtained by evaluating them with different bounded parameter uncertainty ranges and based on three different application requirements.

The rest of the paper is organized as follows: Section II presents the fundamentals of uncertainties and the robustness definition of a control system. Section III presents the proposed robustness evaluation method based on six-sigma. Section IV applies the proposed method to a second-order and DC motor drive systems. Section V applies the proposed robustness evaluation method to PMSM drives, including various RPCs selected from the literature. Section VI highlights the research findings and draws a conclusion.

II. UNCERTAINTIES AND ROBUSTNESS FUNDAMENTALS

Control system uncertainties are mainly generated from differences in plant structure, material and assembly imperfections, friction, environment, and operation changes. To evaluate the effects of uncertainties on the system performance, the uncertainties need to be determined and represented mathematically. For example, parametric uncertainties can be represented and quantified by assuming that each uncertain parameter is bounded within a range. By considering a perturbed uncertain control system, as shown in Fig. 1, that has an uncertain parameter (X_i), unmodelled dynamics uncertainties (Δ_u), the uncertain parameter X_i bounded in a range $X_{min} \leq X_i \leq X_{max}$ can be presented as:

$$X_i = \bar{X} (1 + r_x \Delta) \quad (1)$$

where $\bar{X} = \frac{X_{min} + X_{max}}{2}$ is the mean parameter (nominal) value,

$r_x = \frac{X_{max} - X_{min}}{X_{max} + X_{min}}$ the relative uncertainty in the parameter, and

Δ any real scalar satisfying $|\Delta| \leq 1$. The unmodelled dynamics (Δ_u) with a weight (W_u) and parametric uncertainties can be expressed as lumped uncertainties (G_p) as [29]:

$$G_p = \frac{\bar{X}}{zS + 1} (1 + r_x \Delta) (1 + W_u(s) \Delta_u(s)), \quad (2)$$

$$|\Delta| \leq 1, |\Delta_u(j\omega)| \leq 1 \forall \omega.$$

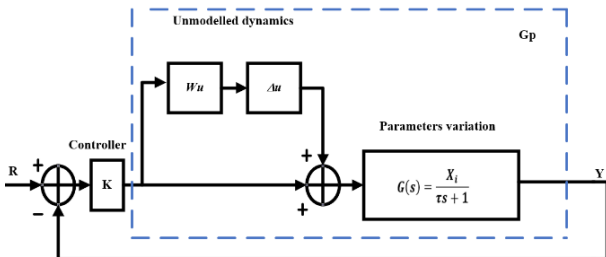


Fig. 1. Perturbed uncertain system [29].

The robustness of a control system, especially in the presence of uncertainties, refers to its capability to preserve specified performance criteria or desired properties within predefined limits, even when subjected to variations or external disturbances [30]. To determine the performance robustness of a control system, the nominal performance has to be obtained first. The maximum and minimum bounds for robustness can then be defined from the nominal point. If system Y has a nominal output Y_0 and the range for robustness within the bounds $[Y_{min}, Y_{max}]$, for any system output Y_i to be robust, it should be within the bounds $[Y_{min}, Y_{max}]$, where:

$$Y_i \xrightarrow{\text{robust}} \text{if } Y_{min} \leq Y_i \leq Y_{max} \quad (3)$$

To illustrate the concept, let us consider the control system shown in Fig. 1 with plant $G(s) = \frac{X_i}{0.5s + 1}$. If the uncertain

parameter X_i of plant $G(s)$ has a nominal value of 4 and varies in the range [1], [7]. By generating a set of step responses, Y_i , with different uncertainties, the nominal response, $Y_{nominal}$, can be first obtained, and the maximum and minimum acceptable responses can be defined as $[Y_{min}, Y_{max}]$. The responses that fall within the acceptable response range are robust, and the other responses outside that range are non-robust, as shown in Fig. 2.

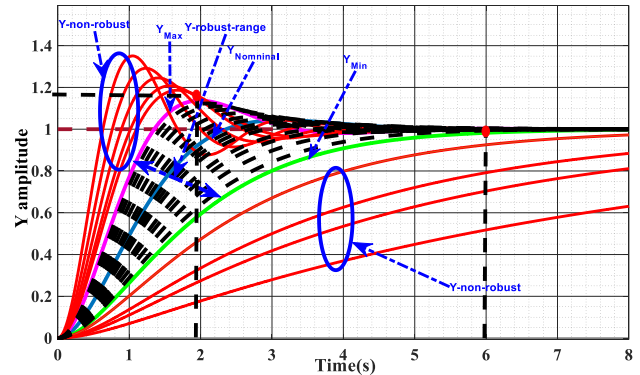


Fig. 2. Robustness range of a simple uncertain feedback control system.

However, this method alone cannot determine the robustness level of a control system. In other words, the variation of output behavior (Y) of a control system with different bounded uncertainties (X_i) still cannot be quantified. Therefore, it is essential to find a statistical robustness evaluation method that can numerically represent a control system's robustness level. The six-sigma robustness evaluation method is introduced to evaluate and quantify the robustness of control systems, which will be discussed in the next section.

III. PROPOSED SIX-SIGMA ROBUSTNESS EVALUATION METHOD

Six-sigma is a quantitative quality measure of a production

process. The term “sigma” basically indicates the standard deviation σ , which measures how a set of data is dispersed around the mean value μ of this data. Considering normally distributed data, the sigma level ($n\sigma$) as the number of defects per million opportunities (DPMO) is presented in Table I. To provide a visual representation, Fig. 3 depicts the normal distribution curves for sigma levels ranging from 1 to 6, assuming a mean value μ of 0, an upper specification limit (USL) of 6, and a lower specification limit (LSL) of -6 . The areas under the normal distribution in Fig. 3 associated with each σ level relate directly to the probability of performance falling in that particular range. For example, σ is equivalent to a probability of 0.683.

Initially, 3σ approach was used, where 3σ is equivalent to the probability of 0.9973 or the POF is 0.27% (2700 defects per million). This probability was deemed acceptable considering short-term (S) quality control. However, in the long term (L), an approximate 1.5σ shift in the mean was experienced, according to MOTOROLA and GE [25]. Due to the 1.5σ shift, the 3σ quality control is insufficient in long term, and thus the 6σ quality control was used to define the long-term sigma quality [31].

TABLE I
SIGMA LEVEL AS PERCENTAGE VARIATION AND DPMO

Sigma level	Percentage variation (%)	DPMO (S)	DPMO (L)
$\pm 1\sigma$	68.26	317 400	697700
$\pm 2\sigma$	95.46	45 400	308733
$\pm 3\sigma$	99.73	2700	66803
$\pm 4\sigma$	99.9937	63	6200
$\pm 5\sigma$	99.999943	0.57	233
$\pm 6\sigma$	99.9999998	0.002	3.4

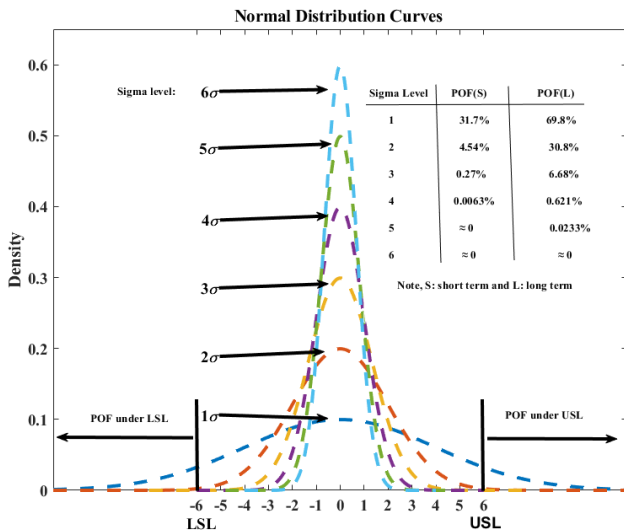


Fig. 3. Normal distribution curves with respect to sigma levels from 1 to 6 under the conditions of $\mu = 0$, $LSL = -6$, and $USL = 6$.

Sigma level is a key property of the six-sigma method that measures the capability of a process to produce defect-free performance. Another important property of the six-sigma method is the Z-value, which measures how many standard deviations, σ , a process specification, X is away from the

mean of the process μ . It calculates the process capability index, which indicates how well the process performs relative to its specifications. The concept of Z-value based on a defined USL is shown in Fig. 4.

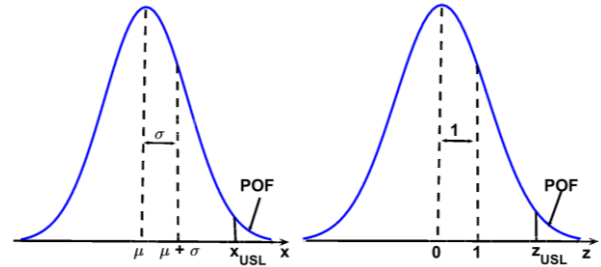


Fig. 4. Normal probability density function (NPDF) and Z_{USL} and its relationship to POF with one-sided hypothesis test for cases with USL.

Six-sigma properties can be used to evaluate and quantify the performance robustness of a control system. First, a system with uncertain parameters (X_c) bounded in predefined range is identified. Then, a set of performance indicators, K_i , that adequately reflects the system performance, and their acceptance levels or upper specification limit, USL_i , are defined. The robustness criteria of the control system with K_i performance indicators, and USL_i specification limits are expressed as:

$$K_i(X_c) \leq USL_i, i = 1, 2, \dots, m \quad (4)$$

where K_i represents the i^{th} performance indicator of a control system, like torque ripple in a motor drive system, e.g., the torque ripple should be less than 0.4 N m.

The Z-value of the i^{th} performance indicator is defined as:

$$Z_i = \frac{USL_i - \mu_i}{\sigma_i}, i = 1, 2, \dots, m \quad (5)$$

where μ_i and σ_i are the mean and standard deviation of the i^{th} performance indicator, respectively.

The Z-value, Z_i , accurately indicates the robustness level of an individual indicator, K_i , relative to the corresponding specification limit, USL_i . However, it is difficult to indicate the overall system robustness using the Z-value for a system with several indicators. Therefore, sigma levels, $n\sigma$, and POFs are used to indicate the overall system robustness. Based on the number of defects, the system, POF_{sys} , can be obtained and used to compute the system sigma level, n_{sys} . For a control system with N samples (total number), if ND is the number of defects, the system's POF and equivalent sigma level can be obtained by [27]:

$$POF_{\text{sys}} = \frac{ND}{N} \quad (6)$$

$$n_{\text{sys}} = \Phi^{-1}\left(1 - \frac{POF_{\text{sys}}}{2}\right) \quad (7)$$

where $\Phi^{-1}(x)$ is the inverse transformation of a standard cumulative distribution function (CDF).

CDF is a mathematical function that maps a random

variable to the probability that the variable is less than or equal to a certain value. In other words, the CDF gives the probability of a random variable X is less than or equal to a specific value x , denoted as $\Phi(x) = \Pr(X \leq x)$. The CDF value is typically in the $[0, 1]$ interval. The inverse CDF generates a random number from a given probability distribution. In contrast, the inverse transform method is a technique used to generate random number from a given probability distribution.

In the six-sigma analysis, the normal distribution is commonly assumed for many processes, although not all processes follow the normal distribution. Several studies suggested data transformation to achieve normality [32] because the process capability measures, e.g., Z -value, require the process data to be normally distributed or can be transformed into the normal distribution data. On the other hand, the equivalent sigma levels, $n\sigma$, can be obtained based on the number of defects (ND) of a process by calculating the percentage of variation (Yield) as follows [33]:

$$\text{Yield\%} = \frac{N - ND}{N} \times 100 \quad (8)$$

The obtained Yield can be used to determine the corresponding sigma level based on the six-sigma conversion table. This method can be applied to any process or control system, regardless of the data distribution [33].

The proposed six-sigma robustness evaluation offers a valuable approach to assessing and quantifying the robustness of control systems. Specifically, it proves useful in evaluating the robustness of control systems that face uncertainties within a bounded range, such as parametric uncertainty. To conduct this evaluation, a set of quality indicators and their corresponding limits are defined. Next, N samples of uncertainties are applied to the control system, and the quality indicators are measured. This step allows for the collection of data on the system's performance under varying uncertainties. Subsequently, statistical measures such as the mean, standard deviation, and number of defects are computed based on the collected data. These measures serve as the foundation for determining Z -values and sigma levels, which provide insights into the system's robustness. Fig. 5 shows the block diagram robustness evaluation process based on six-sigma.

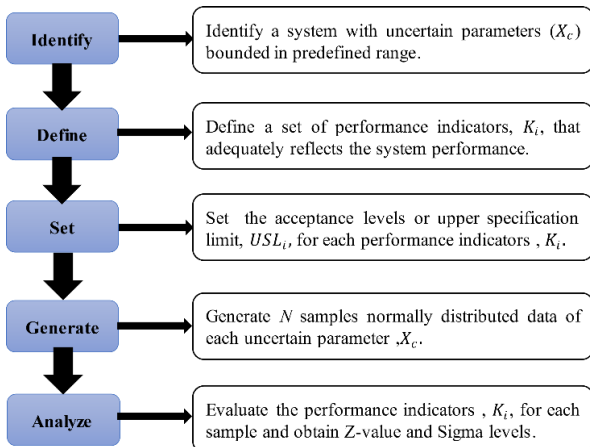


Fig. 5. Block diagram of robustness evaluation process.

IV. CASE STUDY I: SECOND ORDER AND DC DRIVES SYSTEMS

To validate the proposed six-sigma robustness evaluation method, a closed-loop second-order system with uncertain parameters ζ_i and ω_{ni} (Fig. 6) is considered. In order to evaluate the robustness of the stability and performance of the system, some indicators must be defined.

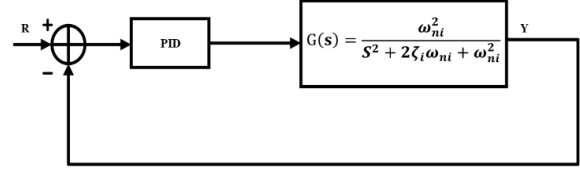


Fig. 6. A second-order closed-loop control system with uncertainties.

The step response characteristics, such as overshoot, OS, settling time, T_s , and root-mean-square error (RMSE), can be used as performance indicators and the location of the real parts of closed-loop poles, P_{CLP} , can be used to indicate stability. Therefore, the performance and stability indicators, K_i , and their upper specification limits, USL_i , are set as constraint functions for an uncertain parameter, X_c , as follows:

$$\begin{bmatrix} \text{RMSE}(X_c) \\ T_s(X_c) \\ \text{OS}(X_c) \\ \text{Re}[P_{CLP}(X_c)] \end{bmatrix} \leq \begin{bmatrix} 0.03 \\ 0.02 \\ 0.04 \\ 0 \end{bmatrix} \quad (9)$$

$\underbrace{\hspace{10em}}_{K_i} \qquad \underbrace{\hspace{10em}}_{USL_i}$

where $X_c = [\zeta_i, \omega_{ni}]$.

To evaluate the robustness numerically, the system is optimized to achieve optimal performance at the nominal values of $\zeta_i=0.6$ and $\omega_{ni}=5$, respectively. Then, four different sets of bounded uncertainty (variation) ranges of ζ_i and ω_{ni} with 10, 000 normally distributed samples (N) for each set are generated randomly. The system is simulated with the generated samples of each set, and the values of performance indicators (T_s , OS, RMSE) and their means μ and standard deviations σ are obtained. The system performance number of defects, ND , are computed as the total times that T_s , OS or RMSE exceed their specification limits. The system stability number of defects, ND , are computed as the total times that the real part of the closed-loop poles ($\text{Re}(P_{CLP})$) is positive. The Z -value of settling time, Z_{T_s} , overshoot, Z_{OS} , and RMSE, Z_{RMSE} , are obtained based on (5), and the sigma level of system performance, n_{sys} , system stability, n_{stab} , and POF of system performance are computed based on (6) and (7), as presented in Table II.

TABLE II
ROBUSTNESS INDEXES OF SECOND ORDER SYSTEM

ω_{ni}	ζ_i	Z_{T_s}	Z_{OS}	Z_{RMSE}	n_{sys}	n_{stab}	POF _{sys}
[3.75,6.25]	[0.45,0.75]	53.4	41.3	114.1	6	6	0
[2.50, 7.50]	[0.30, 0.90]	21.5	17.3	26.0	6	6	0
[1.25, 8.75]	[0.15, 1.05]	4.2	3.7	6.1	3.5	6	0.047%
[0.00,10.00]	[0.00,1.20]	1.4	1.7	2.1	1.2	5	23.014%

The data in Table II indicate a clear relationship between increasing uncertainties and the degradation of the sigma levels associated with system performance and stability. Specifically, as uncertainties increase, the corresponding sigma levels decrease. Notably, the robustness of stability tends to be more resilient to uncertainties compared to performance robustness, with instances where high stability robustness is maintained despite low-performance robustness. The high sigma levels of stability robustness suggest an almost negligible POF of system stability in all cases.

As another example of a more practical system, a DC motor drive system is considered to evaluate its robustness. The following transfer function can represent a DC motor:

$$G(s) = \frac{K_t}{JLs^3 + (JR + BL)s^2 + BRs + K_t^2} \quad (10)$$

where J is the moment of inertia, B the viscous friction constant, K_t the torque constant, R the winding resistance, and L the winding inductance.

The robustness of the DC motor drive can be evaluated similarly to the system shown in Fig. 5. The indicators K_i , and upper specification limits, USLs, are defined as follows:

$$K = \begin{bmatrix} K_1 \\ K_2 \\ K_3 \\ K_4 \end{bmatrix} = \begin{bmatrix} \text{RMSE}(X_c) \\ T_s(X_c) \\ \text{OS}(X_c) \\ \text{Re}[P_{\text{CLP}}(X_c)] \end{bmatrix} \leq \begin{bmatrix} 0.03 \\ 0.04 \\ 0.03 \\ 0 \end{bmatrix} = \text{USL} \quad (11)$$

where $X_c = [R_i, L_i, J_i, B_i]$.

A DC motor drive is optimized to achieve nominal performance with nominal parameters listed in Table III. The robustness evaluation results with three variation ranges of nominal parameters ($\pm 50\%$, $\pm 75\%$, $\pm 100\%$) are shown in Table IV.

TABLE III
NOMINAL DC MOTOR PARAMETERS

Parameter	$R(\Omega)$	$L(\text{H})$	$J(\text{kg m}^2)$	$B(\text{N m s})$	K_t
Value	4	$2.75e^{-6}$	$3.23e^{-6}$	$3.51e^{-6}$	0.0274

TABLE IV
ROBUSTNESS EVALUATION OF DC MOTOR DRIVE WITH PARAMETER UNCERTAINTIES RANGES

Indicator Range	Z_{T_t}	Z_{OS}	Z_{RMSE}	n_{sys}	n_{stab}	POF_{sys}
$\pm 50\%$	26.3	16.7	28.7	6	6	0.0
$\pm 75\%$	6.6	5.1	9.4	4.3	6	0.0017%
$\pm 100\%$	2.5	1.8	2.8	1.6	6	10.96%

The results in Table IV indicate that as the parameter uncertainties increase, the performance of the system deteriorates, and the FOF increases. The robustness of the system's performance is severely affected by parameter uncertainties, where a low sigma level is obtained at high uncertainty ranges. However, the system's stability robustness remains at 6σ across all uncertainty ranges, suggesting that the system's stability is not significantly impacted by parameter uncertainties.

IV. CASE STUDY II: RPCS FOR PMSM DRIVES

A. PMSM Control and Uncertainties

MPC predicts the future states of machine variables based on their current states and mathematical machine models. Based on the controlled variables, model predictive current control (MPCC) and model predictive torque control (MPTC) are the two common MPC methods for PMSM drives. In MPCC, the dq-axis currents i_{dq} , at time instant $k+1$ are predicted as follows:

$$i_d^{k+1} = \left(1 - \frac{R_s T_s}{L_d}\right) i_d^k + \frac{L_q}{L_d} T_s \omega i_q^k + \frac{T_s}{L_d} v_d \quad (12)$$

$$i_q^{k+1} = \left(1 - \frac{R_s T_s}{L_q}\right) i_q^k - \left[\left(\frac{L_d}{L_q} i_d^k + \Psi_{\text{PM}}\right) \omega + \frac{v_d}{L_q} \right] T_s \quad (13)$$

In MPTC, the flux linkage Ψ_{dq} , and torque T_e , at time instant $k+1$ are predicted as follows:

$$\Psi_d^{k+1} = L_d i_d^{k+1} + \Psi_{\text{PM}} \quad (14)$$

$$\Psi_q^{k+1} = L_q i_q^{k+1} \quad (15)$$

$$T_e^{k+1} = \frac{3}{2} p \left[\Psi_{\text{PM}} i_q^{k+1} + (L_d - L_q) i_{dq}^{k+1} \right] \quad (16)$$

where v_d and v_q are the d- and q-axis voltages, i_d and i_q the d- and q-axis currents, respectively, R_s is the stator resistance, L_d and L_q ($L_q = L_d$ in the case of surface-mounted PMSMs) are the d- and q-axis inductances, ω is the machine speed, and Ψ_{PM} the permanent magnet flux in the rotor.

The fundamental principle of MPC is to minimize a cost function that compares the predicted and reference currents for MPCC or torque and flux linkage for MPTC, as the following:

$$g_{\text{MPCC}} = |i_d^* - i_d(k+1)| + |i_q^* - i_q(k+1)| \quad (17)$$

for MPCC, and,

$$g_{\text{MPTC}} = |T_e^* - T_e(k+1)| + \gamma |\Psi_s^* - \Psi_s(k+1)| \quad (18)$$

for MPTC [34], where i_d^* and i_q^* are the reference currents, Ψ_s is the stator flux linkage, $\Psi_s = \Psi_d + j\Psi_q$, Ψ_s^* and T_e^* are the stator flux linkage and torque references, respectively, and γ is the weighting factor.

The MPC of PMSM drives is subject to uncertainties from manufacturing, such as assembly imperfection and PM material diversity, and operation, such as temperature variations and measurement offsets, resulting in unmodelled dynamics and parametric uncertainties [35]. Parametric uncertainty due to machine parameters variation is the most common PMSMs drive uncertainty and severely affects performance [7]. Hence, this research considered only parametric uncertainty.

Generally, PMSM MPC is designed based on an ideal machine model and assuming nominal machine parameters. However, in practice, the machine is never perfect, and the parameters deviate from their nominal values due to

manufacturing tolerances and changes in operating conditions. Thus, to design a control system that can deal with parameter mismatching, it is essential to obtain realistic and practical variation ranges for these parameters by considering the manufacturing tolerances and changes in the operating conditions. Manufacturing tolerance is a specific inaccuracy range in a typical value of a machine variable due to tolerances of geometric dimensions and material properties. Besides, changes in operating conditions include temperature and load changes. For example, the stator resistance R_s depends on the stator temperature. Its nominal value R_{s0} is obtained at 25 °C (room temperature). R_s at operational temperature t (°C) of stator winding can be calculated by:

$$R_s = R_{s0} [1 + \alpha(t - t_0)] \quad (19)$$

where α is a material constant (for copper, $\alpha=0.004 K^{-1}$).

The PM flux linkage, Ψ_{PM} depends on the direct and quadrature axis currents, i_{dq} , and the magnet temperature. The machine inductances L_d and L_q , depend on the currents i_{dq} , and the flux density (slightly affected by machine temperature). In addition, L_d and L_q vary nonlinearly with respect to the load conditions due to magnetic saturation. Mechanical parameters of PMSM also vary during real-time operations. For example, moment inertia J varies when a load is applied to the machine by connecting to an external system. The shape and the dimensions of mechanical loads mainly affect the variation of mechanical parameters. Thus, if the manufacturing tolerance Δ_M , and operational variation Δ_O of a parameter are expressed as a percentage of the nominal values, a parameter variation range can be obtained. For instance, the actual value of R_s can be computed as:

$$R_s = R_0 (1 + \Delta_M(R_0))(1 + \Delta_O(R_0)) \quad (20)$$

If $\Delta_M(R_0) = \pm 10\%$ and $\Delta_O(R_0) = [-5\%, +30\%]$, the uncertainties of R_s can be expressed as:

$$R_s = R_0 [-14.5\%, +43\%] \quad (21)$$

The manufacturing tolerances Δ_M of each parameter depends on the machine manufacturers and what geometric dimensions and materials they used. According to the catalogues of PMSMs manufacturing companies: Windings, Inc. and VEM Group. The typical Δ_M are listed in Table V.

TABLE V
PMSM PARAMETERS MANUFACTURING TOLERANCES (Δ_M)

Parameter Δ_M	R_s	L_d	L_q	Ψ_{PM}	J	B
$\pm\%$	± 10	± 15	± 15	± 10	± 10	± 5

The operational variation Δ_O can be obtained considering two situations (the rated and maximum operating conditions). For example, Δ_O of R_s due to temperature change can be obtained by (19). For a machine with a rated temperature of

70 °C and maximum temperature of 155 °C (class F insulation material), R_s will increase by +18% and +52% of the nominal value at rated and maximum temperature respectively. Also, R_s can be lower than the nominal values at a low temperature before the machine warms up. Thus, minimum -5% and maximum -10% decrease of R_s from the nominal value can be experienced [36].

The potential operational variations of L_d, L_q, Ψ_{PM}, J and B were obtained by investigating several identification methods, such as recursive least-squares (RLS) algorithms, neural networks (NNs), model reference adaptive system (MRAS) based algorithms, online clustering, and particle swarm optimization (PSO) [36]-[41]. The experimental validations of these methods based on different types of PMSMs have found diverse variation ranges of PMSM parameters with changes in operating conditions. For instance, [33] have shown that L_d, L_q and Ψ_{PM} at the full load operation approximately 20%, 35% and 20%, respectively, lower than their actual values at no-load operation.

Different parameter variations are produced up to a certain range depending on the operating conditions. However, it is difficult to operate a motor without damaging it and/or voiding the motor warranty under some conditions. For instance, operating a motor at maximum temperature or torque for an extended period can lead to various types of damage, including electrical, mechanical, and magnetic faults [42]-[43]. Therefore, operational variation ranges of PMSM parameters were obtained based on different identification methods and exaggerated assumptions to cover a wide range of operating conditions [37], as presented in Table VI. Higher operational variation ranges are unlikely to occur in practical situations because the motor may not tolerate extreme operating conditions unless it is practically designed for that [44].

TABLE VI
POTENTIAL OPERATIONAL VARIATIONS OF PMSM PARAMETERS AT RATED & MAXIMUM CONDITIONS

Parameter	Rated condition					
	R_s	L_d	L_q	Ψ_{PM}	J	B
+ %	+30	+10	+15	+5	+15	+10
- %	-5.0	-40	-50	-15	-5	-3.0
Maximum condition						
+ %	+62	+20	+25	+10	+20	+15
- %	-10	-60	-70	-25	-10	-5.0

It is crucial to mention that these ranges of variation were determined by analyzing different studies that used various identification methods and validated them based on interior PMSMs (IPMSMs) or surface-mounted PMSMs (SPMSMs). As a result, these ranges are applicable to both types of motors. However, it is essential to note that these ranges represent potential variations closest to real-world practical condition ranges, and the actual condition ranges may be slightly higher or lower than these values.

Thus, with a percentage variation of Δ_M and Δ_O of each

parameter and using (20), PMSM parameter variation ranges at rated and maximum conditions are listed in Table VII.

TABLE VII
PMSM PARAMETERS POTENTIAL VARIATIONS DUE TO VARIATION OF Δ_M and Δ_O AT RATED & MAXIMUM CONDITIONS

Rated condition						
Parameter Δ	R_s	L_d	L_q	Ψ_{pm}	J	B
+	+43.0	+26.5	+32.3	+15.5	+26.5	+15.5
-	-14.5	-49.0	-57.5	-23.5	-14.5	-7.85
Maximum condition						
+	+78.0	38.0	+43.7	+21.0	+32.0	+20.8
-	-19.0	-66.0	-74.5	-32.5	-19.0	-9.8

B. RPC Methods

To validate and illustrate the proposed six-sigma robustness evaluation based on predictive control of PMSM drives, the conventional MPCC and three existing RPC methods are used to assess their robustness to uncertainties. To evaluate the robustness of RPCs with different robust mechanisms, RPCs based on prediction error correction, disturbance observer, and model-free are considered. The PCC-based prediction error correction proposed in [8] is used and will be referred to as RPC-I. To achieve robustness and compensate for any parameter mismatching, this method uses the weighted errors between the predicted values and measured values in the last sampling instant and adds them to prediction equations in the next sampling instant. MPCC based on an incremental model and disturbance observer proposed in [45] is another RPC to be used and will be referred to as RPC-II. In this method, an incremental prediction model was implemented to eliminate the permanent magnet flux link-age parameter, and an inductance disturbance controller that includes a simple disturbance observer and inductance extraction algorithm was implemented to reduce the effects of machine inductance mismatch. The robust model-free PCC-based current detection technique proposed in [22] is also used and will be referred to as RPC-III. This method works by calculating the difference between the measured currents at different samples. These differences are then used to predict the current in the next sampling. No machine parameters are required for prediction.

B.1 Simulation and Experimental Results

Before evaluating the robustness, the conventional MPC, RPC-I, RPC-II, and RPC-III are validated by numerical simulation and experimental testing. Both controllers are implemented using direct switching (no modulator) and based on the PMSM drive with parameters in Table VIII for a fair comparison. However, to regulate the switching frequency, the switching state changes are limited to no more than one change per control cycle as follows:

$$C_{sw}(k) = \text{Lim}(\Delta S) = \begin{cases} \infty & \text{if } \Delta S > 1 \\ 0 & \text{if } \Delta S \leq 1 \end{cases} \quad (22)$$

where ΔS is the switching pulse change between two cycles

and C_{sw} the switching frequency constraint term.

TABLE VIII
PMSM NOMINAL PARAMETERS

Parameter	Symbol	Value
Stator resistance	R_s/Ω	0.47
d-axis inductance	L_d/mH	14.20
q-axis inductance	L_q/mH	15.90
Permanent magnet flux	Ψ_{pm}/Wb	0.1057
Number of pole pairs	P	3
Inertia	$J/\text{kg m}^2$	0.002
viscous Friction	$B/(\text{N m/rad/s})$	0.0006
DC bus voltage	V_{dc}/V	200
Rated torque	Trated/N m	2
Rated speed	$\omega_{rated}/(\text{r min}^{-1})$	1000
Sampling time	$t_s/\mu\text{s}$	100

The simulation start-up responses from standstill to the rated speed (1000 rpm) with a load torque of 2 N m applied at 0.2 s are shown in Fig. 7. From top to bottom, the graphs are stator current i_a , dq-axis currents i_{dq} , motor torque T_e , and rotor speed ω_r .

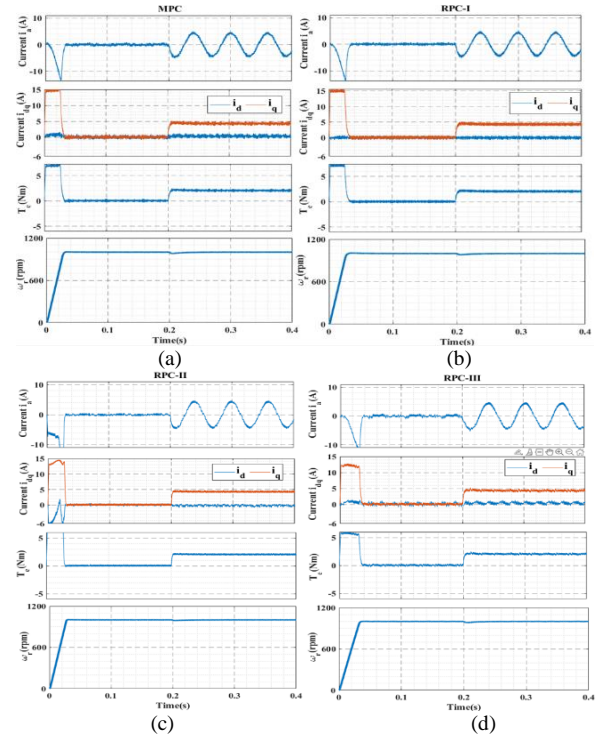


Fig. 7. Simulation start-up performances. (a) MPC. (b) RPC-I. (c) RPC-II. (d) RPC-III.

The simulation results of the MPC and three RPC methods are experimentally validated using a two-level inverter-fed PMSM drive system with the same parameters in Table VI, as shown in Fig. 8. The real-time algorithm is run in a dSPACE DS1104 PPC/DSP control board. A dSPACE Control-Desk interfaced with DS1104 is used for real-time control, monitoring, and recording of experimental results. The motor speed and position are measured by using a 2500-pulse incremental encoder. A Magtrol DSP-6000 programmable dynamometer controller is used to apply the external load.

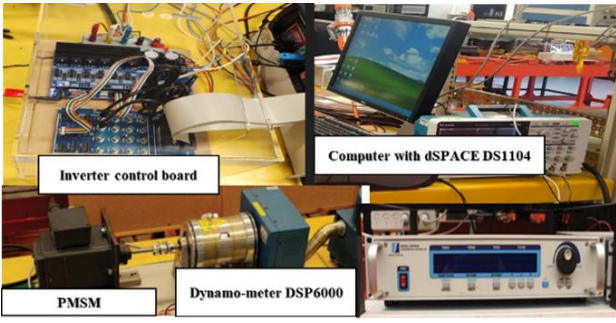


Fig. 8. Experimental setup of PMSM drive system.

The experimental responses during start-up from standstill to rated speed (1000 rpm) are shown in Fig. 9, and the steady-state responses with load torque (2 N m) applied at 0.25 s are shown in Fig. 10. The curves in Figs. 9 and 10 from top to bottom are stator current i_a , d- and q-axis currents i_{dq} , motor torque T_e , and rotor speed ω_r .

Both controllers have shown satisfactory transient and steady-state performances in simulation and experimental tests with nominal machine parameters. The RPC methods have shown better responses than MPC, while their steady-state performances are quite similar. The performance disparities among these controllers arise from their varying robustness techniques. The MPC controller, without any robustness mechanism, suffered the most significant performance degradation. In contrast, RPC-III, which operates without relying on a machine model (model-free), attains remarkable robustness against parameter variations. Moreover, RPC-II eliminates the need for a flux linkage parameter and employs a disturbance observer to enhance its robustness further, resulting in superior performance compared to RPC-I, which relies on the prediction error for robustness improvement.

B.2 Quantitative Analysis

MPC and RPC control methods are quantitatively compared against parametric uncertainties to get a deep insight into the performance differences. The torque and current tracking performances in steady state are measured by computing the torque T_e , stator current i_a , ripples with several parameters variation using the following formula:

$$T_{\text{rip}} = \sqrt{\frac{1}{N} \sum_{i=1}^N [T_e(i) - T_{e\text{avg}}]^2} \quad (23)$$

$$i_{a\text{rip}} = \sqrt{\frac{1}{N} \sum_{i=1}^N [i_a(i) - i_{a\text{ref}}]^2} \quad (24)$$

where, T_{rip} and $i_{a\text{rip}}$ are torque and current ripples, $T_{e\text{avg}}$ and $i_{a\text{ref}}$ are the average torque and reference current, and N is the number of samples used for evaluation.

The MPC and RPC methods are evaluated against parameter variation, where the values of PMSM parameters change in the range of $-\Delta\%$ to $\Delta\%$ of their nominal values (based on Table VII) with the motor operating at 1000 rpm speed and under an external load torque of 2 N m. The steady-state torque and current ripples are computed based on (19)

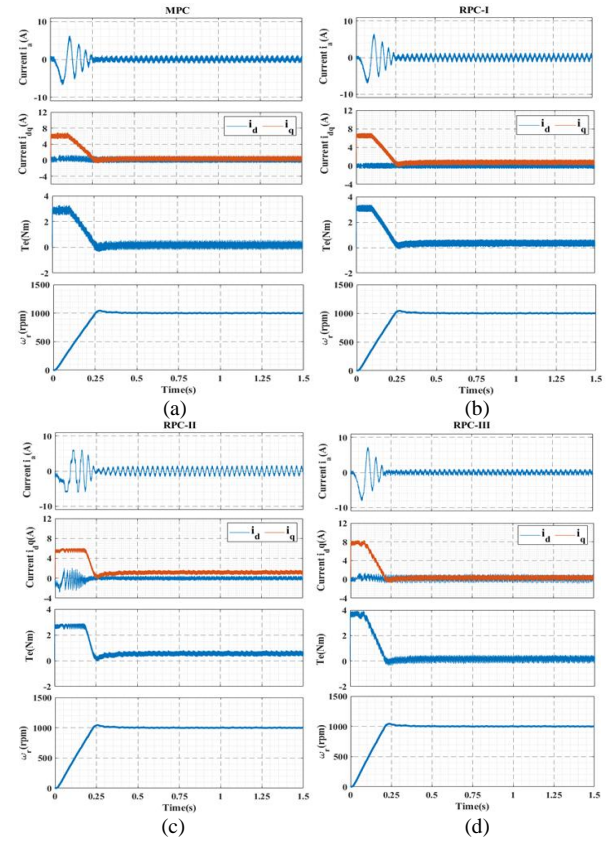


Fig. 9. Experimental transient performances. (a) MPC. (b) RPC-I. (c) RPC-II. (d) RPC-III.

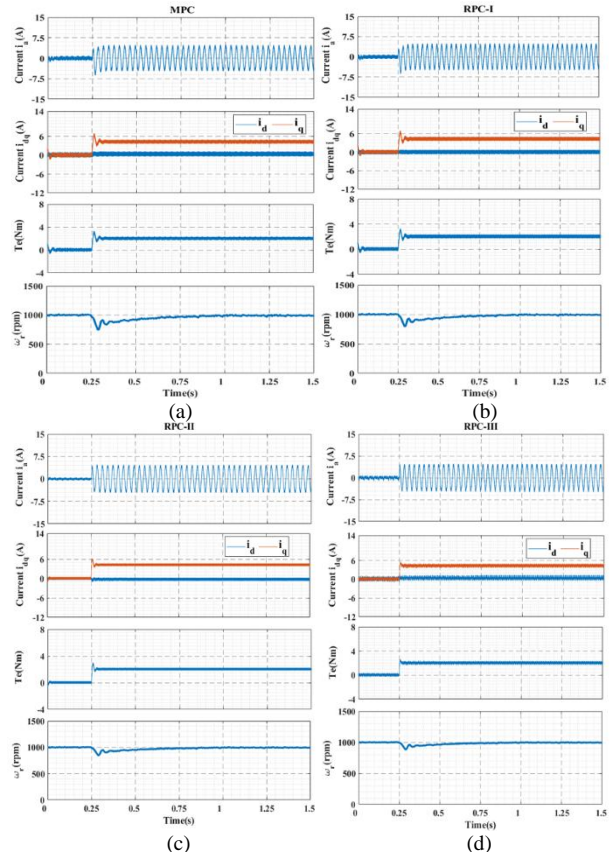


Fig. 10. Experimental steady-state performances. (a) MPC. (b) RPC-I. (c) RPC-II. (d) RPC-III.

and (20). Since the effect of stator resistance R_s , variation is neglectable and the highest effects are produced due to the variations of machine inductances L_q and permanent magnet flux linkage Ψ_{PM} , only ΔL_q and $\Delta \Psi_{PM}$ are considered [45]. Firstly, L_q is varied from -70% to 40% of the nominal value, while the other PMSM parameters are kept at their nominal values. Then, Ψ_{PM} is varied and the other parameters are kept at their nominal values. The torque and current ripples due to the variations of L_q and Ψ_{PM} are shown in Figs. 11.

From the obtained data on torque and current ripples under different parameter variations, it is evident that inductance variation (L_q) has a more significant impact, particularly at lower values, where extremely high ripples are observed. In contrast, variations in permanent magnet flux linkage (Ψ_{PM}) have a comparatively smaller effect, with the highest ripple magnitudes recorded at higher values of Ψ_{PM} . The maximum torque and current ripple values due to inductance variation are observed at -70% ΔL_q for all Ψ controllers. Specifically, when L_q is reduced by 70% , the torque and current ripples increase by 321.8% and 179% for MPC, 280.1% and 205% for RPC-I, 243.9% and 91.4% for RPC-II, and 153.7% and 100.1% for RPC-III compared to their nominal values. However, compared to MPC, the improvements in torque and current ripples are 17.6% and 20.8% for RPC-I, 35.2% and 44.6% for RPC-II, and 57.4% and 61.7% for RPC-III, respectively.

While inductance variations result in an almost linear ripple response for all controllers, the relationship between current ripples and Ψ_{PM} is more complex due to several factors. Changes in Ψ_{PM} influence the back electromotive force, altering current magnitude and leading to non-uniform ripple behavior. Additionally, variations in Ψ_{PM} affect voltage commands, switching patterns, and machine saturation, further distorting ripple characteristics. The sensitivity of different controllers to these variations also contributes to the observed discrepancies.

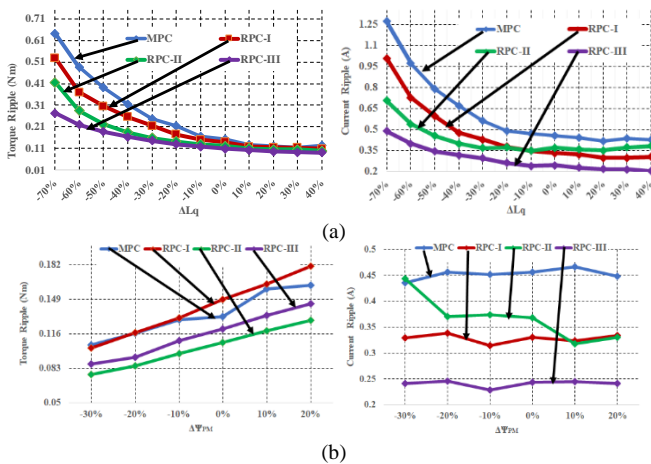


Fig. 11. Current and torque ripples comparison of MPC, RPC-I, RPC-II, and RPC-III with variation. (a) Inductance. (L_q). (b) PM flux linkage (Ψ_{PM}).

RPC methods have shown good responses to parameter variations compared to MPC, which recorded the highest torque and current ripples. RPC-III has shown the best response to parameter variations with smaller current ripples than RPC-I and RPC-II. Thus, it can be concluded that parameter mismatching (uncertainty) can degrade the performance and affect the robustness of PMSM control method.

Evaluating the performance through simulation, experiment, and quantitative analysis with nominal and mismatched machine parameters (as we did in this section) is a commonly used approach for assessing the robustness of MPC and RPCs to uncertainties. This method is often employed in various research studies [22], [24]. Although this approach may provide an initial assessment of RPC performance robustness, it is not always an accurate indication of robustness. The evaluation only considers a limited number of mismatched cases of a single parameter (deterministic approach) and does not precisely determine the robustness level of RPC in the presence of uncertainties. These analyses do not precisely determine how well (robustness level) a drive system performed (compared to other methods) in the presence of uncertainties. To address these limitations, the proposed six-sigma robustness evaluation method is utilized. This approach evaluates RPCs performance robustness with bounded ranges of multiple parameter uncertainties (stochastic approach). By considering multiple parameters and their potential practical variation, the proposed method provides a more accurate and comprehensive evaluation of RPCs' robustness levels.

C. Robustness Evaluation

PMSM drive robustness can be divided into stability robustness and performance robustness. Stability is necessary for performance robustness, meaning the stability robustness level is much larger than the performance robustness level. Therefore, only performance robustness is considered in this evaluation. To evaluate the performance robustness of PMSM drives, performance indicators that essentially indicate the performance quality will be identified [28]. Some of these indicators are step response properties (such as settling time, T_s , and overshoot, OS), and root mean square errors, RMSE, of speed, torque, and current ripples. Then, each indicator's robustness acceptance level (upper specification limit (USL)) needs to be defined. For instance, a torque ripple indicator USL of 0.4 means the torque ripples of a controller must not exceed 0.4 N m over different uncertainties to be considered robust. To select appropriate USLs for all indicators, the requirement of a specific application is considered.

PMSM drives can be used in several applications, such as water-pumping systems, EVs, aircraft flight control, radar systems, and satellites. Each application has different performance requirements, for example, water pumping can operate with low PMSM drive performance, EVs may require moderate drive performance, and applications like radar systems require high drive performance. Thus, the performance indicators K_i with specification limits, USL _{i} ,

considering applications with low requirements (Application-I), moderate requirements (Application-II), and high requirements (Application-III) are listed in Table IX. Therefore, a robustness evaluation model of PMSM drive with K_i performance indicators and their upper specification limits (USL_i) can be defined as follows:

$$K_i = \begin{bmatrix} K_1 \\ K_2 \\ K_3 \\ K_4 \\ K_5 \end{bmatrix} = \begin{bmatrix} T_s(X_c) \\ OS(X_c) \\ RMSE_{\omega}(X_c) \\ T_{rip}(X_c) \\ i_{rip}(X_c) \end{bmatrix} \leq USL_i \quad (25)$$

TABLE IX
PMSM DRIVE PERFORMANCE REQUIREMENTS FOR DIFFERENT APPLICATIONS

Indicator (K_i)	Specification limits (USL_i)		
	Application-I	Application-II	Application-III
T_s	≤ 0.2	≤ 0.15	≤ 0.1
OS	$\leq 5\%$	$\leq 3\%$	$\leq 2\%$
$RMSE_{\omega}$	≤ 0.003	≤ 0.002	≤ 0.001
T_{rip}	≤ 0.8	≤ 0.6	≤ 0.4
i_{rip}	≤ 0.9	≤ 0.7	≤ 0.5

The performance robustness of the conventional MPC and three RPC methods are evaluated for a PMSM drive with nominal parameters (Table VIII) and their uncertainty ranges (Table VII) with $N=10,000$ samples of parameter variations and different application requirements (Table IX) using the proposed six-sigma robustness evaluation method. First, normally distributed machine parameter variation samples are generated for two ranges (rated and maximum conditions). With the motor operating at 1,000 rpm under a 2 N m load torque, the four control methods (MPC, RPC-I, RPC-II, and RPC-III) are evaluated by computing the settling time (T_s), overshoot (OS), RMSE of speed ($RMSE_{\omega}$), torque ripples (T_{rip}), and stator current i_a ripples (i_{rip}) at every parameter variation sample. The number of defects are counted to compute the system POF and sigma level. Also, the mean and standard deviation of each indicator are computed to calculate the Z-values. The robustness evaluation process is illustrated by the flowchart presented in Fig. 12. The Z-values of performance indicators, including settling time, Z_{T_s} , overshoot, Z_{OS} , RMSE of speed, Z_{ω} , torque ripple, $Z_{T_{rip}}$, and current ripple, $Z_{i_{rip}}$, the sigma levels, n_{sys} , and the probabilities of failure of system performance, POF_{sys} , are computed as presented in Table X.

As can be seen from the obtained n_{sys} in Table X, at the rated parameter uncertainty (variation) ranges and application with low requirement (Application-I), all controllers, including MPC, achieved 6σ . With a moderate application requirement (Application-II), MPC and RPC-I only achieved

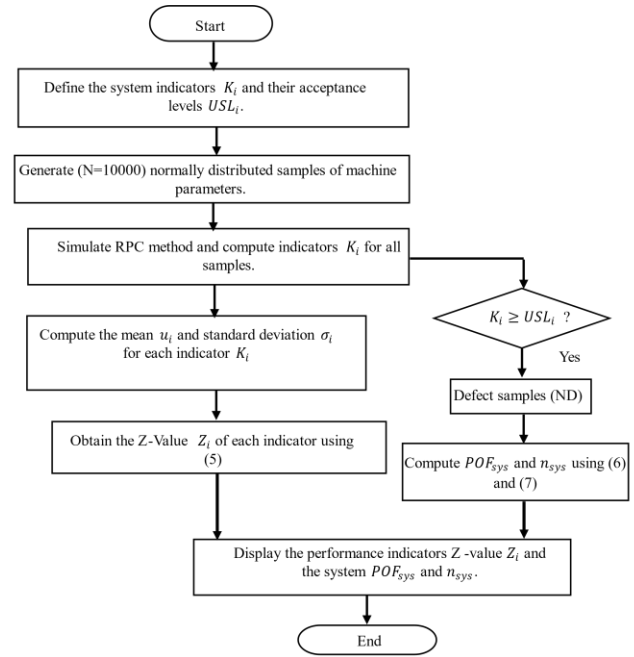


Fig. 12. Flow chart of robustness evaluation process.

2.2σ and 3.6σ , respectively, while other RPC methods achieved 6σ . As for applications with high requirements (Application-III), no controller achieved 6σ , and the highest system sigma level is 2.8σ achieved by RPC-III compared to 0.4σ , 2.0σ , and 2.2σ achieved by MPC, RPC-I, RPC-II, respectively.

At the maximum parameter uncertainty ranges, MPC and RPC-I only achieved 3.1σ and 3.6σ , respectively, and other RPCs achieved 6σ for Application-I. No controller achieved 6σ at maximum parameter uncertainty ranges for moderate and high application requirements, and RPC-III achieved the highest sigma level with 3.8σ and 2.0σ for Application-II and Application-III, respectively. The increase in uncertainty ranges critically influences the robustness, especially for applications with high requirements. For instance, for Application-III, at the maximum uncertainty ranges, low system performance robustness was recorded for MPC, RPC-I, RPC-II, and RPC-III with 100%, 76.65%, 13.36%, and 4.55% POF, respectively. RPC-V achieved the best sigma level and low POF at various uncertainty ranges and for different application requirements.

The current and torque ripples are the most critical performance indicators and the main factor for dropping $n\sigma$ for the overall system. In other words, although some controllers have good robustness for most of the performance indicators, their low robustness levels of torque and/or current ripples result in low $n\sigma$ for overall system performance. In contrast, controllers which maintain trade-offs among torque and current ripples and other performance indicators achieved a good overall system sigma level.

In addition, the Z-value of individual performance indicators is used to show the robustness difference for different controllers, especially when multiple controllers achieve a similar system's sigma level. The Z-value describes

TABLE X

ROBUSTNESS EVALUATION OF MPC, RPC-I, RPC-II, AND RPC-III:
Z-VALUES, SIGMA LEVELS, AND POF UNDER DIFFERENT UNCERTAINTY
RANGES AND APPLICATION REQUIREMENTS

Indicator	Z_{T_s}	Z_{OS}	Z_{ω}	$Z_{T_{rip}}$	$Z_{i_{rip}}$	n_{sys}	POF
Rated condition uncertainties (application-I)							
MPC	65.1	68.1	56.2	17.2	9.3	6.0	0
RPC-I	75.6	214	179.1	19.1	15.1	6.0	0
RPC-II	75.9	167.1	125.8	29.6	25.3	6.0	0
RPC-III	84.6	55.2	52.4	36.5	26.6	6.0	0
Maximum condition uncertainties (application-I)							
MPC	48.2	56	31.6	10.5	5	3.2	0.14%
RPC-I	57.2	168.1	114.3	11.8	8.3	3.7	0.02%
RPC-II	57.4	108.8	85.4	19.1	16	6.0	0
RPC-III	63.2	53.6	45.2	21.6	14.7	6.0	0
Rated condition uncertainties (application-II)							
MPC	45.7	39.6	36.1	11.7	2.2	2.3	2.14%
RPC-I	53.4	124.5	117.1	13	5.6	3.1	0.19%
RPC-II	53.6	98.6	81.5	17.5	8.7	6.0	0
RPC-III	60.4	32.5	32.3	25.5	10.3	6.0	0
Maximum condition uncertainties (application II)							
MPC	33.6	32.5	20.1	7.1	0.9	1.6	10.96%
RPC-I	40.3	97.8	74.7	8	2.8	2.4	1.64%
RPC-II	40.5	64.1	55.4	11.2	5.3	3.3	0.10%
RPC-III	45.1	31.6	27.8	15	5.4	3.8	0.01%
Rated condition uncertainties (application-III)							
MPC	26.3	25.4	16.1	6.2	-0.6	0.5	61.71%
RPC-I	31.3	79.8	55.2	7	1.8	2.1	3.57%
RPC-II	31.4	64.3	37.1	5.2	2.1	2.3	2.14%
RPC-III	36.2	21.2	12.2	14.5	3.8	2.9	0.37%
Maximum condition uncertainties (application-III)							
MPC	19.2	20.8	8.8	3.7	-0.7	0.4	70.85%
RPC-I	23.4	62.6	35.1	4.5	0.7	1.5	13.36%
RPC-II	23.5	41.8	25.1	3.1	1	1.6	10.96%
RPC-III	26.8	20.6	10.5	8.4	1.7	2.1	3.57%

how far the specification limits of each application are from the average value of the N -sample data of each performance indicator. The Z values of torque and current ripples are the most critical indicators for a controller's robustness. Thus, to illustrate the concept of Z -value, the process capability of the torque and current ripple indicators with rated and maximum uncertainty ranges are shown in Fig. 13. USL-I, USL-II, and USL-III, and Z .USL-I, Z .USL-II, and Z .USL-III are the specification limits (Table IX) and Z -values for applications I, II, and III, respectively.

The process capability plots show how far the specification limits positions of different applications from the mean (μ) of torque and current ripples of each controller. The dispersion of torque and current ripples around the mean (μ) shows how good each controller is in maintaining minimum torque or current ripples with parameter variations. For example, the process capability plots of current ripples illustrate how good RPC-III is in maintaining low current ripples over different parameter variations.

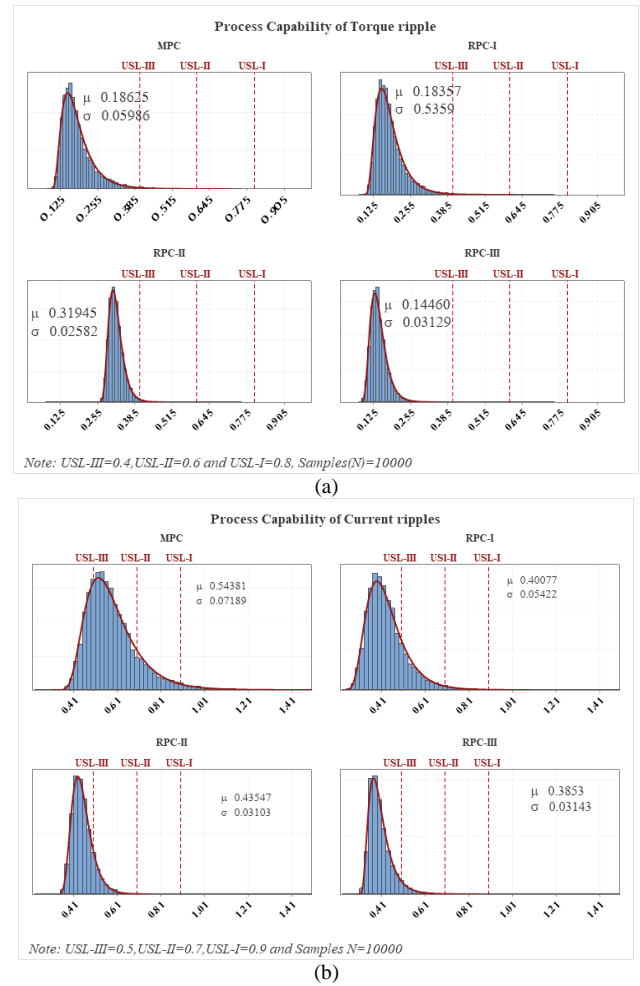


Fig. 13. Process capability plots for MPC, RPC-I, RPC-II, and RPC-III with maximum parameter uncertainty ranges. (a) Torque ripples (T_{rip}). (b) Current ripple (i_{rip}).

The Z -values of different performance indicators show the strengths and weaknesses of different controllers to specific indicators and which controller can maintain a robustness trade-off among all indicators. For instance, MPC and RPC-I have achieved good speed performance robustness (T_s , OS, RMSE $_{\omega}$), but they were unable to maintain good torque and current (T_{rip} , i_{rip}) robustness over different parameter uncertainty ranges. On the other hand, RPC-II and RPC-III may have achieved less overshoot robustness than MPC and RPC-I, but they maintained a robustness trade-off with other indicators, thus achieving higher system sigma levels.

While the robustness evaluation results in Table X provide valuable insight into the robustness of different current controllers to parameter variations, it is important to note that the MPC and RPC methods maintain the same outer speed controller settings and only differ in the current controller designs. Therefore, the proposed robustness evaluation method mainly assesses the robustness of different current controllers to parameter variations, rather than the overall performance of the control scheme. The obtained sigma levels, POFs and Z -values give a comprehensive robustness assessment of different current controllers to the variations of PMSM machine parameters. For instance, model-free

predictive current controller (RPC-III) is more robust than other current controllers under the variation of different machine parameters.

The proposed six-sigma robustness evaluation method offers a simple and reliable robustness evaluation tool applicable to any control system. The robustness level of a control system can be determined by evaluating its quality indicators against defined acceptance levels (specification limits) for N samples of uncertainties. When considering a specific application requirement (e.g., EV), the best controller that is more robust to uncertainties can be selected effectively. The control methods and the application requirements used in this research are just examples to illustrate the proposed six-sigma robustness evaluation method. However, other control methods for PMSM drives, systems, and application performance requirements can be used. Hence, the proposed method is a quality measure of a control system that can be used to numerically assess the robustness of any control system to uncertainties.

VI. CONCLUSION

This paper proposed a robustness evaluation method based on the six-sigma concept for evaluating the performance robustness of PMSM control systems against parameter uncertainties. This method is applicable to other control systems. A simple second-order system, DC motor drive, and four predictive control methods of PMSM drives were investigated to validate the proposed method. From the obtained evaluation results, the following conclusions can be drawn:

Firstly, the sigma level and Z-values of a control system are inversely proportional to the system uncertainties. Since the range of stability robustness is much wider than that of performance robustness, robust stability is a requirement for robust performance. This is clearly shown in the evaluation results of the second-order system, where in some cases, low sigma levels of system performance were recorded while 6σ system stability was achieved.

Secondly, the system sigma level of a controller is influenced by the robustness of all performance indicators. Thus, a high system sigma level is recorded for controllers that maintain robustness trade-off among different indicators, as illustrated by the evaluation data of MPC and RPC methods. For instance, RPC-III may have achieved less overshoot robustness than RPC-I but was able to keep balance with torque and current ripple robustness and, thus, achieved a sigma level higher than other controllers.

For future works, the system stability robustness, and other uncertainties, e.g., unmodeled dynamics, will be investigated for robust PMSM drives. Additionally, different methods will be explored to reduce the sample size of the evaluation and simplify the calculation process.

REFERENCES

- [1] R. Fales, "Uncertainty Modeling and Predicting the Probability of Stability and Performance in the Manufacture of Dynamic Systems," *ISA transactions*, vol. 49, no. 4, pp. 528–534, Oct. 2010.
- [2] K.-Z. Liu, and Y. Yao, *Robust Control: Theory and Applications*. John Wiley & Sons, 2016.
- [3] N. Farah, G. Lei, and J. G. Zhu *et al.*, "Two-vector Dimensionless Model Predictive Control of PMSM Drives based on Fuzzy Decision Making," *CES Transactions on Electrical Machines and Systems*, vol. 6, no. 4, pp. 393–403, Dec. 2022.
- [4] Z. Y. Liu, T. Fan, and G. L. He *et al.*, "Research on High-performance Explicit Model Predictive Control Algorithm for Permanent Magnet Synchronous Motors," *Transactions of China Electrotechnical Society*, vol. 38, no. 22, pp. 6039–6058, 2023.
- [5] J. J. Ren, Y. Q. Ye, and G. F. Xu *et al.*, "Uncertainty-and-disturbance-estimator-based Current Control Scheme for PMSM Drives with a Simple Parameter Tuning Algorithm," *IEEE Trans. on Power Electr.*, vol. 32, no. 7, pp. 5712–5722, Jul. 2017.
- [6] L. L. Guo, P. S. Wang, and Y. Y. Li *et al.*, "Visual Analysis of Parameters Mismatch in Model Predictive Control for Permanent Magnet Synchronous Motor under Different Cost Functions," *Transactions of China Electrotechnical Society*, vol. 38, no. 4, pp. 903–914, 2023.
- [7] J. Yang, W. H. Chen, and S. H. Li *et al.*, "Disturbance/Uncertainty Estimation and Attenuation Techniques in PMSM Drives—A Survey," *IEEE Trans. on Ind. Electr.*, vol. 64, no. 4, pp. 3273–3285, Apr. 2017.
- [8] M. Siami, D. A. Khaburi, and A. Abbaszadeh *et al.*, "Robustness Improvement of Predictive Current Control Using Prediction Error Correction for Permanent-magnet Synchronous Machines," *IEEE Trans. on Ind. Electr.*, vol. 63, no. 6, pp. 3458–3466, Jun. 2016.
- [9] F. X. Wang, K. K. Zuo, and P. Tao *et al.*, "High Performance Model Predictive Control for PMSM by using Stator Current Mathematical Model Self-regulation Technique," *IEEE Trans. on Power Electr.*, vol. 35, no. 12, pp. 13652–13662, Dec. 2020.
- [10] Y. F. Li, Y. Li, and Q. Wang, "Robust Predictive Current Control with Parallel Compensation Terms Against Multi-parameter Mismatches for PMSMs," *IEEE Trans. on Energy Conversion*, vol. 35, no. 4, pp. 2222–2230, Dec. 2020.
- [11] Y. S. Hu, C. G. Hu, and P. J. Zhang *et al.*, "A Novel Hybrid Seven-level Converter for Permanent Magnet Synchronous Motor Driving System based on Model Predictive Control," *CES Trans. on Electr. Mach. and Sys.*, vol. 3, no. 4, pp. 389–396, Dec. 2019.
- [12] S.-W. Kang, J.-H. Soh, and R.-Y. Kim *et al.*, "Robust Predictive Current Control for IPMSM Without Rotor Flux Information based on a Discrete-time Disturbance Observer," *IET Electric Power Applications*, vol. 13, no. 12, pp. 2079–2089, Dec. 2019.
- [13] X. Fang, L. M. Wang, and K. Zhang, "High Order Nonsingular Fast Terminal Sliding Mode Control of Permanent Magnet Linear Motor based on Disturbance Observer," *Transactions of China Electrotechnical Society*, vol. 38, no. 2, pp. 409–421, 2023.
- [14] M. Yang, X. Y. Lang, and J. Long *et al.*, "Flux Immunity Robust Predictive Current Control with Incremental Model and Extended State Observer for PMSM Drive," *IEEE Trans. on Power Electr.*, vol. 32, no. 12, pp. 9267–9279, Dec. 2017.
- [15] Y. P. Zhang, Z. G. Yin, and M. Su *et al.*, "Unified Full Speed Sensorless Control of Interior Permanent Magnet Synchronous Motor based on Resonance Extended State Observer," *Transactions of China Electrotechnical Society*, vol. 38, no. 22, pp. 6070–6081, 2023.
- [16] F. X. Wang, L. He, and J. Rodriguez, "FPGA based Continuous Control Set Model Predictive Current Control for PMSM System Using Multi-step Error Tracking Technique," *IEEE Trans. on Power Electr.*, vol. 35, no. 12, pp. 13455–13464, Dec. 2020.
- [17] S. G. Mei, W. Z. Lu, and Q. G. Fan *et al.*, "Sensorless Control Strategy of Permanent Magnet Synchronous Motor based on Error Compensation Estimated by Sliding Mode Observer," *Transactions of China Electrotechnical Society*, vol. 38, no. 2, pp. 398–408, 2023.
- [18] W. Xie, X. C. Wang, and F. X. Wang *et al.*, "Finite-control-set Model Predictive Torque Control with a Deadbeat Solution for PMSM Drives," *IEEE Trans. on Ind. Electr.*, vol. 62, no. 9, pp. 5402–5410, Sept. 2015.
- [19] Y. Liu, S. M. Cheng, and B. W. Ning *et al.*, "Robust Model Predictive Control with Simplified Repetitive Control for Electrical Machine Drives," *IEEE Trans. on Power Electr.*, vol. 34, no. 5, pp. 4524–4535, May 2018.
- [20] Y. N. Zhou, H. M. Li, and H. G. Zhang, "Model-free Deadbeat Predictive Current Control of a Surface-mounted Permanent Magnet

- Synchronous Motor Drive System,” *J Power Electr.*, vol. 18, no. 1, pp. 103–115, 2018.
- [21] Z. Sun, Y. T. Deng, and J. L. Wang *et al.*, “Finite Control Set Model-Free Predictive Current Control of PMSM With Two Voltage Vectors Based on Ultralocal Model,” *IEEE Trans. on Power Electr.*, vol. 38, no. 1, pp. 776–788, Jan. 2023.
- [22] C. K. Lin, T. H. Liu, and J. T. Yu *et al.*, “Model-free Predictive Current Control for Interior Permanent-magnet Synchronous Motor Drives based on Current Difference Detection Technique,” *IEEE Trans. on Ind. Electr.*, vol. 61, no. 2, pp. 667–681, Feb. 2014.
- [23] C. W. Ma, J. Rodriguez, and C. Garcia *et al.*, “Integration of Reference Current Slope Based Model-free Predictive Control in Modulated PMSM Drives,” *IEEE J. of Em. and Sel. Top. in Power Electr.*, vol. 11, no. 2, pp. 1407–1421, Apr. 2023.
- [24] L. Ortombina, P. Karamanakos, and M. Zigliotto, “Robustness Analysis of Long-horizon Direct Model Predictive Control: Permanent Magnet Synchronous Motor Drives,” in *Proc. of 2020 IEEE 21st Workshop on Control and Modeling for Power Electronics (COMPEL)*, Aalborg, Denmark, 2020, pp. 1–8.
- [25] P. N. Koch, R.-J. Yang, and L. Gu, “Design for Six Sigma Through Robust Optimization,” *Struct. and Multidisc. Optim.*, vol. 26, no. 3, pp. 235–248, 2004.
- [26] G. Lei, J. G. Zhu, and Y. G. Guo, *Multidisciplinary Design Optimization Methods for Electrical Machines and Drive Systems* (Power Systems). 1st ed. Berlin Heidelberg: Springer, 2016.
- [27] C.-S. Jun, and B.-I. Kwon, “Process Capability Control Procedure for Electrical Machines by Using a Six-sigma Process for Achieving Six-sigma Quality Level,” *IET Electric Power Applications*, vol. 11, no. 8, pp. 1466–1474, Sept. 2017.
- [28] N. Farah, G. Lei, and J. G. Zhu *et al.*, “Robust Model-free Reinforcement Learning Based Current Control of PMSM Drives,” *IEEE Trans. on Transp. Electr.*, vol. 11, no. 1, pp. 1061–1076, Feb. 2025.
- [29] S. Skogestad, and I. Postlethwaite, *Multivariable Feedback Control: Analysis and Design*. 2nd ed. Wiley-Interscience, 2005.
- [30] K. M. Zhou, and J. C. Doyle, *Essentials of Robust Control*. Prentice hall Upper Saddle River, NJ, 1997.
- [31] G. Lei, T. S. Wang, and J. G. Zhu *et al.*, “System-level Design Optimization Method for Electrical Drive Systems—Robust approach,” *IEEE Trans. on Ind. Electr.*, vol. 62, no. 8, pp. 4702–4713, Aug. 2015.
- [32] T. Aldowaisan, M. Nourelfath, and J. Hassan, “Six Sigma Performance for Non-normal Processes,” *European Journal of Operational Research*, vol. 247, no. 3, pp. 968–977, Dec. 2015.
- [33] Council for Six Sigma Certification, Craig Joseph Setter, *Six Sigma: A Complete Step-by-step Guide: A Complete Training & Reference Guide for White Belts, Yellow Belts, Green Belts, and Black Belts*. The Council for Six Sigma Certification, Buffalo, WY, Harmony Living, LLC, 2018, pp. 9–22.
- [34] Y. C. Zhang, D. L. Xu, and J. L. Liu *et al.*, “Performance Improvement of Model-predictive Current Control of Permanent Magnet Synchronous Motor Drives,” *IEEE Trans. on Ind. Appl.*, vol. 53, no. 4, pp. 3683–3695, Jul.-Aug. 2017.
- [35] T. M. Jahns, and W. L. Soong, “Pulsating Torque Minimization Techniques for Permanent Magnet AC Motor Drives—A Review,” *IEEE Trans. on Ind. Electr.*, vol. 43, no. 2, pp. 321–330, Apr. 1996.
- [36] E. M. Tofghi, A. Mahdizadeh, and M. R. Feyzi, “Real-time Estimation and Tracking of Parameters in Permanent Magnet Synchronous Motor Using a Modified Two-stage Particle Swarm Optimization Algorithm,” in *Proc. of 2013 IEEE International Symposium on Sensorless Control for Electrical Drives and Predictive Control of Electrical Drives and Power Electronics (SLED/PRECEDE)*, Munich, Germany, 2013, pp. 1–7.
- [37] C. Y. Lai, G. D. Feng, and K. Mukherjee *et al.*, “Investigations of the Influence of PMSM Parameter Variations in Optimal Stator Current Design for Torque Ripple Minimization,” *IEEE Trans. on Energy Conversion*, vol. 32, no. 3, pp. 1052–1062, Spt. 2017.
- [38] X. D. Liu, H. Chen, and J. Zhao *et al.*, “Research on the Performances and Parameters of Interior PMSM Used for Electric Vehicles,” *IEEE Trans. on Ind. Electr.*, vol. 63, no. 6, pp. 3533–3545, Jun. 2016.
- [39] G. D. Feng, C. Y. Lai, and K. Mukherjee *et al.*, “Current Injection-based Online Parameter and VSI Nonlinearity Estimation for PMSM Drives Using Current and Voltage DC Components,” *IEEE Trans. on Transp. Electr.*, vol. 2, no. 2, pp. 119–128, Jun. 2016.
- [40] Z. Q. Zhu, D. Wu, and W. Q. Chu, “On-load Performance in IPM Machines Having Different Slot/pole Number Combinations Considering Local Magnetic Saturation,” in *Proc. of 2016 IEEE Vehicle Power and Propulsion Conference (VPPC)*, Hangzhou, China, 2016, pp. 1–6.
- [41] M. Koç, and O. Emre Özçiflikçi, “Precise Torque Control for Interior Mounted Permanent Magnet Synchronous Motors with Recursive Least Squares Algorithm Based Parameter Estimations,” *Engineering Science and Technology, an International Journal*, vol. 34, p. 101087, Oct. 2022.
- [42] J. M. Zheng, Z. H. Wang, and D. X. Wang *et al.*, “Review of Fault Diagnosis of PMSM Drive System in Electric Vehicles,” in *Proc. of 2017 36th Chinese Control Conference (CCC)*, Dalian, China, 2017, pp. 7426–7432.
- [43] P. Pietrzak, and M. Wolkiewicz, “Demagnetization Fault Diagnosis of Permanent Magnet Synchronous Motors based on Stator Current Signal Processing and Machine Learning Algorithms,” *Sensors (Basel)*, vol. 23, no. 4, p. 1757, Feb. 2023.
- [44] M. Thiele, *Analysis of Cogging Torque Due to Manufacturing Variations in Fractional Pitch Permanent Magnet Synchronous Machines*. Charles Darwin University (Australia), 2013.
- [45] X. G. Zhang, L. Zhang, and Y. C. Zhang, “Model Predictive Current Control for PMSM Drives with Parameter Robustness Improvement,” *IEEE Trans. on Power Electr.*, vol. 34, no. 2, pp. 1645–1657, Feb. 2019.



Nabil Farah, Nabil Farah (Graduate Student Member, IEEE) received the bachelor’s and master’s degrees in electrical engineering from University Teknikal Malaysia Melaka, in 2015 and 2018, respectively, and the Ph.D. degree in electrical engineering from the University of Technology Sydney (UTS), in 2024. He is currently a Research Associate at UTS and a Lecturer at Melbourne Institute of Technology (MIT), Sydney. His research interests include electrical machine drive control and optimization, predictive control, and machine learning methods for PMSM drives.



Gang Lei (M’14-SM’22) received a B.S. degree in Mathematics from Huanggang Normal University, China, in 2003, an M.S. degree in Mathematics, and a Ph.D. degree in Electrical Engineering from Huazhong University of Science and Technology, China, in 2006 and 2009, respectively. He is currently a Senior Lecturer at the School of Electrical and Data Engineering, University of Technology Sydney (UTS), Australia. His research interests include computational electromagnetics, design optimization, and control of electrical drive systems and renewable energy systems. He is an Associate Editor of the IEEE Transactions on Industrial Electronics and the IEEE Transactions on Energy Conversion.



Jianguo Zhu (S'93-M'96-SM'03) received a B.E. degree in 1982 from Jiangsu Institute of Technology, Jiangsu, China, an M.E. degree in 1987 from Shanghai University of Technology, Shanghai, China, and a Ph.D. degree in 1995 from the University of Technology Sydney (UTS), Sydney, Australia, all in electrical engineering. He was appointed a lecturer at UTS in 1994, promoted to full professor in 2004, and Distinguished Professor of Electrical Engineering in 2017. He has held various leadership positions, including Head of the School for Electrical, Mechanical, and Mechatronic Systems and director of the Centre for Electrical Machines and Power Electronics Director at UTS and Head of the School for Electrical and Information Engineering at the University of Sydney (USyd), Australia. He is now a full professor at USyd. His research interests include computational electromagnetics, characterization of magnetic properties of materials, electrical machines and drives, power electronics, renewable energy systems, and smart grids.



Youguang Guo (Senior Member, IEEE) received a B.E. degree from Huazhong University of Science and Technology, Wuhan, China, in 1985, the M.E. degree from Zhejiang University, Hangzhou, China, in 1988, and the Ph.D. degree from the University of Technology Sydney (UTS), Sydney, NSW, Australia, in 2004, all in electrical engineering. He is currently a Professor at the School of Electrical and Data Engineering, UTS. His research fields include the measurement and modeling of properties of magnetic materials, numerical analysis of the electromagnetic field, electrical machine design optimization, and power electronic and drives.